Monte Carlo Simulations of Asymmetric Diblock Copolymer Thin Films Confined between Two Homogeneous Surfaces

Qiang Wang, Paul F. Nealey, and Juan J. de Pablo*

Department of Chemical Engineering, University of Wisconsin−Madison, Madison, Wisconsin 53706-1691

Received October 31, 2000; Revised Manuscript Received February 9, 2001

ABSTRACT: We report the first Monte Carlo simulations of the morphology of asymmetric diblock copolymer thin films confined between two homogeneous and identical surfaces. The copolymers form a cylindrical morphology in the bulk. Exploratory bulk simulations have been conducted with judicious choices of the simulation box dimensions to find the characteristic periodicity of the cylinders. The morphological dependence of the thin films on the surface−block interactions and the film thickness has then been systematically investigated. Our results are in good agreement with experimental observations.

1. Introduction

Block copolymers are known to self-assemble into microphase-separated domains on the scale of tens of nanometers at temperatures below the order−disorder transition (ODT).[1] Recently, thin films of block copolymers have received considerable attention because of their potential applications in nanofabrication.[2] Control of morphology in the films, including the orientation and ordering of block copolymer domains, is essential for some applications such as nanolithography. In thin films, the surface−block interactions and the confinement give rise to morphologies that differ from those in the bulk. By understanding thin-film morphologies at a fundamental level, the control of morphology could conceivably be achieved by finely tuning the surface−block interactions and the film thickness.

The morphology of symmetric diblock copolymers confined between two homogeneous surfaces has been extensively studied experimentally,[3−8] by simulations,[9−13] and theoretically.[14−26] The use of stripe-patterned surfaces has also been investigated[27−39] to enhance the formation of long-range ordered (in the plane of the film) perpendicular lamellae, which are desirable for some lithographic processes. Remarkably, only a few theoretical studies[16,40,41] have considered the morphology of confined *asymmetric* diblock copolymers, and no simulations have been reported. Here we present the first results of Monte Carlo simulations of the morphology of confined films of asymmetric diblock copolymers; the copolymers exhibit a cylindrical bulk morphology. In the following discussion, we denote the minority component as A and the majority component as B. Accordingly, the surface energetically preferring A blocks is referred to as the "sA surface", and the surface energetically preferring B blocks is referred to as the "sB surface".

For completeness, we summarize in Table 1 the morphologies that have been reported from some experiments[42−49] of thin films of asymmetric diblock copolymers having a cylindrical bulk morphology. These experiments are for supported films with a free surface (e.g., air) or free-standing films. Note that due to the complexity of the system in question, it is difficult to precisely describe with the simple notation of Table 1 the experimental morphologies in great detail; some morphologies were not even clearly identified in the experiments. Furthermore, in some cases detailed comparisons between different experimental systems may not be too meaningful. Table 1 is only used to provide an overview of what has been reported in these experiments, and a *qualitative* comparison with our simulation results shown below. For details about the observed morphologies in the experiments, readers are referred to the original publications. In addition to the work listed in Table 1, the thin-film morphology of cylinder-forming asymmetric diblock copolymers was studied in recent experiments by Lammertink et al.[50,51] and Thurn-Albrecht et al.[52]

From Table 1 we can see that all the substrates and the free surfaces employed in these experiments exhibit a preference for one of the two blocks. This preference generally leads to cylinders of A blocks parallel to the surfaces (denoted by the symbol $C_{||}^{n}$, where n is the number of cylinder layers). In some cases, one layer of half-cylinders parallel to the surfaces (observed near the surfaces, denoted by $C_{||}^{1/2}$) and perpendicular cylinders (denoted by $C_{\perp}$) have also been observed. In addition, noncylindrical morphologies have been observed in all the experiments, including lamellae where planar A−B interfaces parallel to the surfaces are observed (denoted by $L_{||}$ for each A−B lamella), a layer of hexagonally packed spheres of A blocks parallel to the surfaces (denoted by S), and perforated lamellae of A blocks parallel to the surfaces where hexagonally arranged B-rich holes are observed (denoted by P for each layer). These noncylindrical morphologies are caused by the surface preference and the confinement. We note that in these experiments the $L_{||}$ morphology has been consistently observed near an sA surface but not near an sB surface.[53] This will be discussed in detail in section 4.

Only a few theoretical studies have been reported on the morphology of confined films of asymmetric diblock copolymers having a cylindrical bulk morphology. Using a Cahn−Hilliard formalism, Brown and Chakrabarti[16] performed two-dimensional numerical calculations of asymmetric diblock copolymers with a volume fraction

* To whom correspondence should be addressed.

10.1021/ma0018751 CCC: $20.00
Published on Web 04/06/2001

Table 1. Summary of Observed Morphologies in Some Experiments on Thin Films of Asymmetric Diblock Copolymers Having a Cylindrical Bulk Morphology[a]

Reference	Diblock Copolymer A-B (kg/mol)	L_0 (nm)	Surfaces (Lower-Upper)	Observed Morphology
[42]	PB-PS (10/23)	34.6	sA-sA	$L_{\|}$-$L_{\|}$ (*Peripheral region*)
				$L_{\|}$-$C_{\|}^{1}$-$L_{\|}$
				$L_{\|}$-$C_{\|}^{2}$-$L_{\|}$
				$L_{\|}$-$C_{\perp}$-$L_{\|}$ (Thickest part of some droplets where $D \geq 150$nm)
[43]	PEE-PEP	53.7	sA-sA	$C_{\|}^{1/2}$-$L_{\|}$ (D=49nm)
				$L_{\|}$-$C_{\|}^{3}$-$L_{\|}$ (D=185nm)
				$L_{\|}$-$C_{\|}^{n}$-$L_{\|}$ (D=640nm. An isotropic orientation of cylinders in the middle of the film is gradually reached as approaching from the surfaces)
[44]	PVP-PS		sA-sB	$L_{\|}$-$C_{\|}^{1}$&S (D=53nm)
				$L_{\|}$-$C_{\|}^{2}$&$C_{\perp}$ (D=100.2nm)
				$L_{\|}$-$C_{\|}^{n}$&$C_{\perp}$ (D=200.8nm)
[45]	PB-PS (10/23)	34.6	sA-sA	$L_{\|}$-$C_{\|}^{1}$-$L_{\|}$ ($D \approx 50$nm)
				$L_{\|}$-$C_{\perp}$-$L_{\|}$ (D=100~150nm)
[46]	PS-PB (10/23)	21.9	sB-sB	P (*Minimum thickness region*, D=25~27nm)
				$C_{\|}^{2}$ or P-P (*First terrace*)
				$C_{\|}^{n}$
	PB-PS (10/23)	34.6	sA-sA	$L_{\|}$-$L_{\|}$ (*Minimum thickness region*, D=18~21nm)
				$L_{\|}$-S-$L_{\|}$
				$L_{\|}$-$C_{\|}^{1}$-$L_{\|}$ (*First terrace*, D=33~35nm)
				$L_{\|}$-$C_{\|}^{n}$-$L_{\|}$
[47]	PB-PS (11/36)		sA-sA	$L_{\|}$-$L_{\|}$ (0^{th} *layer*, D=30nm)
				$L_{\|}$-S-$L_{\|}$ (For thickness a few nanometer thinner than the 1^{st} *layer* shown below)
				$L_{\|}$-$C_{\|}^{1}$-$L_{\|}$ (1^{st} *layer*, D=50nm)
			sB-sA	$L_{\|}$ (0^{th} *layer*, D=15nm)
				S-$L_{\|}$ (For thickness a few nanometer thinner than the 1^{st} *layer* shown below)
				$C_{\|}^{1}$-$L_{\|}$ (1^{st} *layer*, D=35nm)
[48]	PB-PS (11/36)		sA-sA	$L_{\|}$-$L_{\|}$ (0^{th} *layer*, D=30nm)
				$L_{\|}$-S-$L_{\|}$ (For thickness a few nanometer thinner than the 1^{st} *layer* shown below)
				$L_{\|}$-$C_{\|}^{1}$-$L_{\|}$ (1^{st} *layer*, D=50nm)
				$L_{\|}$-$C_{\|}^{2}$-$L_{\|}$ (D=70nm)
			sB-sA	$C_{\|}^{n}$-$L_{\|}$ (D=240nm, $n \approx 11$)
[49]	PB-PS (11/36)		sA-sA	$L_{\|}$-$C_{\|}^{2}$-$L_{\|}$ (D=70nm)
				$L_{\|}$-P-S-$L_{\|}$ (At the edge of islands of D=90nm shown below)
				$L_{\|}$-$C_{\|}^{3}$-$L_{\|}$ (D=90nm)

[a] All the experiments are for thin films having at least one free surface. The *shorter* blocks are denoted by A, and the *longer* blocks are denoted by B. Accordingly, the surface energetically preferring A blocks is referred to as the sA surface, and the surface energetically preferring B blocks is referred to as the sB surface. The diblock copolymers are denoted as A−B in the second column, where PB denotes poly(butadiene), PS is poly(styrene), PEE is poly(ethylethylene), PEP is poly(ethylene−propylene), and PVP is poly(vinylpyridine). The numbers in parentheses following the copolymers, e.g. 10/23, represent the molecular weight of the A/B blocks in units of kg/mol. L_0 denotes the intercylinder distance in the bulk. In the last column, different symbols denote different morphologies: $C_{\|}^{n}$ denotes the cylinders of A blocks parallel to the surfaces, where n is the number of cylinder layers; $C_{\|}^{1/2}$ denotes one layer of half-cylinders parallel to the surfaces (observed near the surfaces); $C_{\perp}$ denotes perpendicular cylinders; $L_{\|}$ denotes one A−B lamella having a planar A−B interface parallel to the surfaces; S denotes one layer of spheres of A blocks parallel to the surfaces; P denotes one layer of perforated lamellae of A blocks (with B-rich holes) parallel to the surfaces. The symbol & denotes the coexistence of two morphologies. For example, $L_{\|}$−$C_{\|}^{1}$&S represents the morphology of $L_{\|}$ near the lower surface and the coexistence of $C_{\|}^{1}$ and S near the upper surface. D denotes the film thickness. Different morphologies reported in each study under a certain surface configuration are listed from top to bottom with increasing D. Phrases in italic font in parentheses following the morphology, e.g., *peripheral region*, are the terminology used in the corresponding reference for a certain film thickness.

of the *shorter* blocks (denoted by f_A) of 0.33. The copolymers were confined between two hard surfaces: a lower sB surface preferring the *longer* blocks through a long-range potential and an upper neutral surface. After a deep quench, lamellar-like structures were found near the preferential surface, while the A component formed circular domains packed in a somewhat irregular hexagon throughout the rest of the film.[16] Suh et al.[40] used a phenomenological theory to study the parallel and perpendicular orientations of cylinders confined between two identical surfaces in the strong segregation limit. Their results showed that perpendicular cylinders can occur in thin films (less than a few intercylinder distances in thickness) if the difference between the two surface−block interfacial tensions is small. Huinink et al.[41] employed a dynamic density functional theory to study asymmetric diblock copolymers with $f_A = {}^1/_3$ confined between two identical

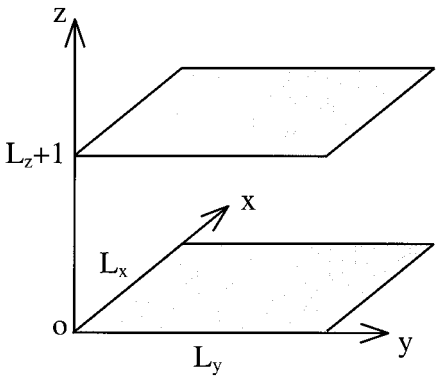

Figure 1. Surface configuration for confined films. The two surfaces are homogeneous and identical; they can be sA (energetically repelling B blocks), sB (energetically repelling A blocks), or neutral surfaces.

surfaces. The surfaces were neutral or preferred B blocks. They investigated the morphology dependence on the film thickness and the strength of the surface preference. Different morphologies, namely $C_{||}^{n}$, $C_{\perp}$, $L_{||}$, and P, were observed in their work.[41] Their results will be discussed and compared with our simulations in section 4.

In this work, we perform extensive Monte Carlo simulations of asymmetric diblock copolymers confined between two identical, hard and homogeneous surfaces. Such simulations are carried out in an expanded grand-canonical ensemble; the confined films are in thermodynamic equilibrium with a bulk phase having a specified chemical potential and temperature corresponding to a cylindrical morphology. We focus on the morphological dependence of the thin films on the film thickness and the surface preference. This paper is organized as follows: In section 2 we briefly describe the model and the simulation methodology. In section 3 we present a method to estimate the characteristic periodicity of the bulk morphology from exploratory simulations. In section 4 we present our simulation results for confined films. The last section is devoted to conclusions.

2. Model

Our Monte Carlo simulations are performed in an expanded grand-canonical ensemble in the framework of a simple cubic lattice. The model employed here is the same as that employed in ref 13, where a detailed description can be found. Only a brief account is given here.

2.1. Simple Cubic Lattice Model. In the simple cubic lattice model, an asymmetric diblock copolymer chain consists of N segments. The first N_A segments are of type A, and the rest are of type B. Each segment occupies one lattice site, and each lattice site is occupied by at most one segment. A rectangular simulation box of dimensions L_x, L_y, and L_z is employed. To simulate a confined film, two flat and homogeneous surfaces are introduced through the lattice sites at $z = 0$ and $z = L_z + 1$, respectively, as shown in Figure 1. To represent hard surfaces, these lattice sites are not allowed to be occupied by polymer segments. Diblock copolymers are therefore confined to a thin-film geometry of thickness $D = L_z - 1$. Periodic boundary conditions (PBC) are imposed in the x and y directions. For simulations in the bulk, PBC are also imposed in the z direction.

In our model, we only consider repulsions between nonbonded nearest-neighbor A−B pairs separated by one lattice unit ($\epsilon_{A-B} > 0$), and we set $\epsilon_{A-A} = \epsilon_{B-B} = 0$. Interactions between vacancies (unoccupied lattice sites) and polymer segments are also set to zero. Three kinds of sites populate the surfaces: sA, sB, and sN, whose nature depends on the type of surface−block interactions. For simplicity, we set $\epsilon_{sN-A} = \epsilon_{sN-B} = \epsilon_{sA-A} = \epsilon_{sB-B} = 0$ and $\epsilon_{sA-B} > 0$, $\epsilon_{sB-A} > 0$. Therefore, a homogeneous surface consisting of sN sites is neutral, with no *energetic* preference for either of the two blocks. A homogeneous surface consisting of sA sites repels B segments and is therefore preferential to A segments (sA surface), and vice versa. The strength of the surface preference is defined as $\alpha \equiv \epsilon_{sA-B}/\epsilon_{A-B}$ for the sA surface and $\alpha \equiv \epsilon_{sB-A}/\epsilon_{A-B}$ for the sB surface. For a neutral surface $\alpha = 0$. Following our previous work,[13,30,31] $\alpha = 0.5$ corresponds to a weakly preferential surface and $\alpha = 2$ corresponds to a strongly preferential surface.

2.2. Simulations in an Expanded Grand-Canonical Ensemble. We perform Monte Carlo simulations in a variant of the expanded grand-canonical ensemble method proposed by Escobedo and de Pablo.[54] The chemical potential and temperature of the simulated system are specified prior to a simulation. The confined copolymers are therefore in thermodynamic equilibrium with a bulk phase having the same chemical potential and temperature, and the density of the system is allowed to fluctuate during the simulation. In addition to molecule displacements by reptation moves and local (kink-jump and crankshaft) moves, we employ growing/shrinking moves to gradually insert/remove particles from the system.[13] These moves are performed with m_A segments of type A and, simultaneously, m_B segments of type B. To preserve a constant composition of the asymmetric diblock copolymers, defined as $f_A \equiv N_A/N$, we require $m_A/(m_A + m_B) = f_A$. To facilitate transitions, configurational bias is used for these growing/shrinking moves,[13] leading to an acceptance rate of about 40% for our system with $m_A = 1$. A standard Metropolis algorithm is employed in our simulations. One Monte Carlo step (MCS) consists of $0.7 \times L_x \times L_y \times L_z$ trials of reptation, local, and growing/shrinking moves, each of which occurs with the same probability. In general, we discard the first 500 000 MCS (or more) for equilibration and then make a run of at least 1 500 000 MCS (500 000 MCS for bulk simulations) while collecting data every 5 MCS.

We study asymmetric diblock copolymers with $N = 36$ and $f_A = {}^1/_4$. We set the reduced temperature to be $T^* \equiv k_B T/\epsilon_{A-B} = 1.5$, where k_B is Boltzmann's constant and T is the absolute temperature. We also set the reduced chemical potential at $\mu^* \equiv \mu/(k_B T) = 46$, where μ is the chemical potential of the system. These conditions lead to densities (percentage of occupied lattice sites) of $\rho \approx 0.7$, corresponding to highly concentrated copolymer solutions or melts.[55] In a series of bulk simulations we estimated the ODT of the copolymers to be around $T^* = 3.0$. Well-ordered, hexagonally packed cylinders of A in a matrix of B blocks are observed in all of our bulk simulations at $\mu^* = 46$ and $T^* = 1.5$. An example is shown in Figure 2.

2.3. Characterization of Morphology. To identify a morphology in simulations of confined films, in addition to visual inspection of configurations, we also calculate the following ensemble-averaged profiles along the z direction (perpendicular to the surfaces). Note that

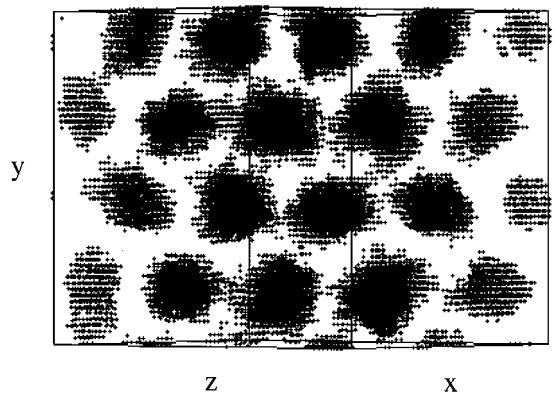

Figure 2. Representative configuration of a bulk simulation at $\mu^* = 46$ and $T^* = 1.5$ for a box with dimensions $54 \times 56 \times 63$. Only A segments are shown as dots. Well-ordered, hexagonally packed cylinders of A in a matrix of B blocks are observed in the bulk simulation. The cylinders are viewed along their axis, which is parallel to the $x-z$ plane but not the x or z axis.

one configuration corresponds to one microstate of the system, and we collect at least 300 000 configurations during a simulation run; the ensemble-averaged profiles are therefore more meaningful and conclusive for characterization of different morphologies than visual inspection.

2.3.1. Density Profile and Order Parameter Profile. The density profile is denoted by $\langle\rho(z)\rangle$, where $\rho(z)$ is the percentage of occupied lattice sites in the cross section of the $x-y$ plane at a given z in each configuration, and $\langle\ \rangle$ represents an average over all the collected configurations (after equilibration). It has been consistently observed in simulations[9,13] that, to reduce the interfacial energy of the system, vacancies segregate to A−B interfaces as well as the surfaces (for repulsive surface−block interactions). Since different morphologies exhibit different A−B interface shapes, the segregation of vacancies leads to different density profiles, which can be used to identify a morphology.

The order parameter profile is defined as $\langle\rho_A(z) - \rho_B(z)\rangle$, where, for each configuration, $\rho_A(z)$ ($\rho_B(z)$) is the percentage of lattice sites occupied by A (B) segments in the cross section of the $x-y$ plane at a given z.[13,30]

2.3.2. Orientation Profiles of Diblock Copolymer Chains. To describe the orientation of a copolymer chain, we define an orientation vector pointing from the center-of-mass of an A block to the center-of-mass of a B block on the same molecule.[13,30] Since we are only concerned with the orientation of chains relative to the surfaces, we calculate $\langle|\cos\theta(z)|\rangle_g$ and $\langle\cos\theta(z)\rangle_g$, where $0 \le \theta(z) \le \pi$ is the angle between the direction of the z axis and the orientation vector of a chain whose center-of-mass (for the whole chain) is located between $z - 0.5$ and $z + 0.5$ ($z = 1, 2, ..., L_z$); $\langle\ \rangle_g$ is an average over all such chains in each collected configuration and over 1000 successively collected configurations (5000 MCS in our simulations). Such an average can therefore provide qualitative and "instantaneous" information about some locally stable morphology.

If chains are mainly parallel to the surfaces, then $\theta(z) \approx \pi/2$, $\langle|\cos\theta(z)|\rangle_g \approx 0$, and $\langle\cos\theta(z)\rangle_g \approx 0$. If chains are mainly perpendicular to the surfaces, $\theta(z) \approx 0$ or π, $\langle|\cos\theta(z)|\rangle_g \approx 1$, and $\langle\cos\theta(z)\rangle_g \approx 1$ (in the case of $\theta(z) \approx 0$) or -1 (in the case of $\theta(z) \approx \pi$). Because of morphology irregularities, we choose $\langle|\cos\theta(z)|\rangle_g = (1/\pi)\int_0^\pi|\cos\theta|\ d\theta = 2/\pi$ as the criterion between the perpendicular and parallel orientations of the chains. This quantity is represented by a dotted line in the figures of chain orientation profiles.

2.3.3. Center-of-Mass Distributions of Diblock Copolymer Chains. We also calculate center-of-mass distributions along the z direction for A blocks, B blocks, and the whole chain. They are denoted by $\langle C_A(z)\rangle_g$, $\langle C_B(z)\rangle_g$, and $\langle C(z)\rangle_g$, respectively. For example, for a given configuration, $C_A(z) \equiv L_z N_{C,A}(z)/N_c$, where $N_{C,A}(z)$ is the number of chains whose A block center-of-mass lies between $z - 0.5$ and $z + 0.5$ ($z = 1, 2, ..., L_z$), N_c is the total number of chains in the system,[13] and L_z is used to rescale the distribution so that a uniform distribution gives $C_A(z) = 1$.

2.3.4. Distributions of Chain Ends and A-Joint Segments. Similarly, we calculate the distributions of chain ends of type A and B and the A-joint segments (the A segments that are bonded to B segments) along the z direction, denoted by $\langle E_A(z)\rangle_g$, $\langle E_B(z)\rangle_g$, and $\langle J_A(z)\rangle_g$, respectively. For example, for a collected configuration, $E_A(z) \equiv L_z N_{E,A}(z)/N_c$, where $N_{E,A}(z)$ is the number of chains whose A-end lies at z ($z = 1, 2, ..., L_z$).

3. Simulations in the Bulk

For constant-volume simulations of block copolymers below the ODT, as pointed out in our previous work,[13] an appropriate match between the periodic boundary conditions (PBC) imposed on the simulation box and the characteristic periodicity of the microphase-separated structure is crucial to obtain meaningful results. In general, the characteristic periodicity of a bulk phase (the "true" value achieved when the simulation box is infinitely large) is unknown and must be determined from exploratory simulations in finite-size boxes with PBC. The problem is that PBC quantize the possible periodicity of an ordered structure in a (finite) simulation box, thereby leading to unusual finite size effects.[56] One obvious way of reducing finite size effects is to use larger box sizes (volumes), at the expense of considerable computational resources. Unfortunately, simulations in large boxes where finite size effects are negligible are beyond current computational capabilities. In small systems, where the box size is only a small multiple of the characteristic periodicity of a pattern (which is the case for *all* the Monte Carlo and molecular dynamics simulations of block copolymers in the literature), the box dimensions can influence significantly the resulting morphology and even frustrate it.[13] In general, rectangular boxes with $L_x \neq L_y \neq L_z$ have greater commensurability with a lamellar or a hexagonal pattern than boxes with two or three equal sides. This provides us with another way of reducing finite size effects. That is, we use boxes whose dimensions facilitate the formation of periodic structures that resemble the bulk morphology.

The box dimensions must be judiciously chosen so that they provide the system with as many different periodicities as possible for a given morphology. (Each periodicity corresponds to a specific orientation of the ordered structure relative to the box frame of reference.) As mentioned above, because of PBC, these periodicities are the only "options" available to the system in the simulation box; the more "options", the better. Furthermore, these "options" should be nearly uniformly distributed in the range where the "true" periodicity is estimated to lie. Because of the large energy barriers between configurations having different orientation, in

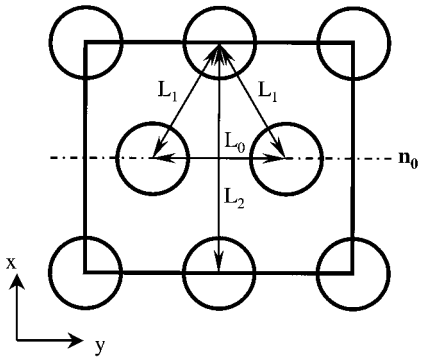

Figure 3. Matching hexagonally packed cylinders with a rectangular box. The *z* direction, which is also the axis of the cylinders, is perpendicular to the paper. Therefore, the axis of the cylinders is parallel to both the $x-z$ and $y-z$ surfaces of the box. We require that the two L_1 be equal and that $L_0 - 1 < L_1 < L_0 + 1$. For a *regular*-hexagonal arrangement of cylinders, $L_1 = L_0$ and $L_2 = \sqrt{3}L_0$.

a simulation run the system is often unable to visit more than one orientation. However, the periodicity corresponding to the orientation observed in a run is usually close to the "true" one, since the system has a tendency to reach its "true" periodicity even in a finite box. In our work, several runs leading to different "observed" periodicities are conducted, and the "true" periodicity is determined from the distribution of these "observed" values. This idea was previously used to estimate the bulk lamellar period in our simulations of symmetric diblock copolymers.[13]

The two-dimensional hexagonal arrangement of cylinders in the bulk places severe constraints on the selection of box dimensions. For hexagonally packed cylinders, we can use the axis of the cylinders to represent their orientation. If the axis of the cylinders is not parallel to any of the $x-y$, $y-z$, and $x-z$ surfaces of the simulation box, it would in general be difficult to match in 3D the rectangular box with the hexagonal pattern of the cylinders. We therefore only consider orientations where the axis of the cylinders is parallel to one (e.g., the case of Figure 2) or two surfaces (e.g., the case of Figure 3) of the box. We now concentrate on the plane perpendicular to the axis of the cylinders. As shown in Figure 3, to further characterize the hexagonal pattern in this plane, we define $\mathbf{n}_0$, a vector in the plane, as the direction connecting the centers of two nearest cylinders. We require that $\mathbf{n}_0$ be parallel to one surface of the box (this surface must be parallel to the axis of the cylinders). For example, in Figure 2 $\mathbf{n}_0$ is parallel to the $x-z$ surface of the box, and in Figure 3 it is parallel to the $y-z$ surface of the box. Again, for our purposes we disregard the orientations for which $\mathbf{n}_0$ cannot be defined according to these criteria. (That would in general be the case if we rotate the hexagonal pattern of cylinders shown in Figure 3 around the *z* axis by an arbitrary angle.) The problem at hand is therefore reduced to that of matching in 2D a rectangle with a hexagon where $\mathbf{n}_0$ is parallel to one side of the rectangle.

As shown in Figure 3, we define L_0 as the distance between the centers of two nearest cylinders that are in the direction of $\mathbf{n}_0$, and L_1 as the distance between the centers of two nearest cylinders that are *not* in the direction of $\mathbf{n}_0$. There are two values of L_1, corresponding to two different directions. We further require that the cylinders be packed in a way such that these two values of L_1 are equal; i.e., the centers of any three closest

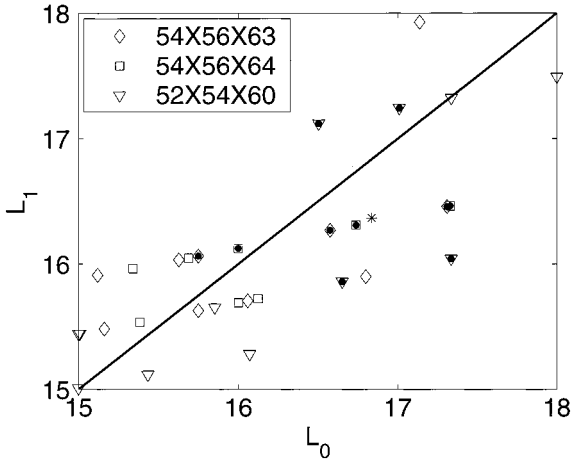

Figure 4. Bulk simulation results for different boxes. Open symbols with different shapes represent the possible periodicities of hexagonally packed cylinders in the corresponding boxes given in the legend. The filled circles represent "observed" periodicities in our bulk simulations. The asterisk represents the average periodicity. The diagonal represents the *regular*-hexagonal packing of cylinders.

Table 2. Comparison of the Mean-Square End-to-End Distances of the Whole Chain, A Block, and B Block in Different Morphologies

	$\langle d^2_{EE}\rangle$	$\langle d^2_{EE,A}\rangle$	$\langle d^2_{EE,B}\rangle$
disordered state in bulk ($\epsilon_{A-B} = 0$)	56.92	11.76	42.21
hexagonally packed cylinders in bulk ($T^* = 1.5$)	76.99	12.54	46.18
$L_{\|\|}-L_{\|\|}$ between sA−sA surfaces ($D/L_2 = 0.5$, $\alpha = 2$)	71.90	11.31	47.79
P between sB−sB surfaces ($D/L_2 = 0.5$, $\alpha = 2$)	68.94	12.31	41.96

cylinders form an isosceles triangle. Therefore, the pattern period in the direction perpendicular to $\mathbf{n}_0$, denoted by L_2 (which crosses two layers of cylinders), can be calculated as $L_2 = (4L_1^2 - L_0^2)^{1/2}$. In a *regular*-hexagonal pattern of cylinders, the centers of any three closest cylinders form an equilateral triangle, and therefore $L_1 = L_0$ and $L_2 = \sqrt{3}L_0$.

When the axis of the cylinders is parallel to two surfaces of the box (e.g., the case of Figure 3), the rectangle is just the cross section of the box in the plane perpendicular to the axis of the cylinders. In this case, since $\sqrt{3}$ is an irrational number while the box dimensions in lattice simulations must be integers, it is not possible to match a *regular* hexagon (where $L_1 = L_0$) with the rectangle. Therefore, we slightly relax the condition for a *regular*-hexagonal structure of cylinders to one in which $L_0 - 1 < L_1 < L_0 + 1$. (We expect $L_0 =$ 15−18 for our system.)

After the above simplifications, three different boxes ($54 \times 56 \times 63$, $54 \times 56 \times 64$, and $52 \times 54 \times 60$) are chosen since they have more "options" to capture the cylindrical morphology (as shown in Figure 4), and they have reasonable sizes ($L_x \times L_y \times L_z < 200\,000$). We performed a total of 15 bulk simulation runs with these boxes at $T^* = 1.5$ and $\mu^* = 46$ and obtained 10 different orientations (and different L_0 and L_1) of the cylinders. (Some runs with the same box and different random number generator seeds resulted in the same orientation.) The results are shown in Figure 4. We obtained the average values of $L_0 \approx 16.8$ and $L_1 \approx 16.4$. Similar to our bulk simulations for symmetric diblock copolymers,[13] the scatter in our results is due to the large

Table 3. Summary of the Morphologies Observed in Our Simulations of Asymmetric Diblock Copolymers Confined between Two Homogeneous and Identical Surfaces[a]

D/L_2	sB-sB				sN-sN	sA-sA		
	2	1	0.5	0.2	0	0.5	1	2
0.5	P	P	P	$C_\perp$	$C_\parallel^{1/2}$-$C_\parallel^{1/2}$	$L_\parallel$-$L_\parallel$	$L_\parallel$-$L_\parallel$	$L_\parallel$-$L_\parallel$
0.75	--	--	$C_\perp$	$C_\perp$	$C_\perp$	$L_\parallel$-S-$L_\parallel$	$L_\parallel$-S-$L_\parallel$	$L_\parallel$-S-$L_\parallel$
1	P-P	P-P	$C_\parallel^2$ (16.05)	$C_\perp$	$C_\parallel^{1/2}$-$C_\parallel^1$-$C_\parallel^{1/2}$	$L_\parallel$-P-$L_\parallel$	$L_\parallel$-P-$L_\parallel$	$L_\parallel$-P-$L_\parallel$
1.25	$C_\parallel$-$C_\perp$-$C_\parallel'$	$C_\parallel$-$C_\perp$-$C_\parallel'$	$C_\perp$	$C_\perp$	$C_\perp$	--	$L_\parallel$-$C_\parallel^1$-$L_\parallel$ (14.32)	$L_\parallel$-$C_\parallel^1$-$L_\parallel$ (14.32)
1.5	$C_\parallel^3$ (16.05)	--	$C_\parallel^3$ (16.31)	$C_\perp$	$C_\parallel^{1/2}$-$C_\parallel^2$-$C_\parallel^{1/2}$	$L_\parallel$-$C_\parallel^2$-$L_\parallel$ (16.05)	$L_\parallel$-$C_\parallel^2$-$L_\parallel$ (16.05)	$L_\parallel$-$C_\parallel^2$-$L_\parallel$ (16.05)
1.75	$C_\parallel$-$C_\perp$-$C_\parallel'$	$C_\parallel$-$C_\perp$-$C_\parallel'$	$C_\perp$	$C_\perp$	$C_\perp$	$L_\parallel$-$C_\parallel^2$-$L_\parallel$ (16.05)	$L_\parallel$-$C_\parallel^2$-$L_\parallel$ (16.05)	$L_\parallel$-$C_\parallel^2$-$L_\parallel$ (16.05)
2	$C_\parallel^4$	$C_\parallel^4$	$C_\parallel^4$	$C_\perp$	$C_\parallel^{1/2}$-$C_\parallel^3$-$C_\parallel^{1/2}$	$L_\parallel$-$C_\parallel^3$-$L_\parallel$ (16.05)	--	$L_\parallel$-$C_\parallel^3$-$L_\parallel$ (16.05)
3	--	--	--	$C_\perp$	$C_\parallel^{1/2}$-$C_\parallel^5$-$C_\parallel^{1/2}$	--	--	--

[a] The strength of surface preference α for each column is listed in the second row. Refer to Table 1 for explanation of the morphologies. In addition, $C_\parallel$−$C_\perp$−$C_\parallel'$ represents the mixed morphology of perpendicular cylinders ($C_\perp$) in the interior of the film and one layer of parallel cylinders ($C_\parallel$ and $C_\parallel'$) near each surface (formed by the interconnection of A domains at a small distance away from the surfaces). The number in parentheses is the intercylinder distance (parallel to the surfaces) of $C_\parallel^n$ that is reduced from L_0. The symbol - - represents that no simulations have been conducted under the corresponding surface configurations.

energy barriers that separate configurations with different orientations. Such barriers are difficult to overcome during a single simulation run.

We also calculated the mean-square end-to-end distances for the whole chain, the A block, and the B block (denoted by $\langle d_{EE}^2 \rangle$, $\langle d_{EE,A}^2 \rangle$, and $\langle d_{EE,B}^2 \rangle$, respectively) from our bulk simulations. Their average values are listed in Table 2. We can see that *all* of them are larger than the corresponding values in the athermal ($\epsilon_{A-B} = 0$) case, showing that chains are stretched in the ordered phase.

4. Simulations of Confined Films

We study thin films confined between two identical and homogeneous surfaces, as shown in Figure 1. We vary the strength of surface preference α from 0 (neutral) to 2 (strongly preferential)[13] and the film thickness D from 14 ($0.5L_2$) to 84 ($3L_2$). The sides $L_x \times L_y$ are chosen as 28 × 34 ($L_2 \times 2L_0$) or 56 × 67 ($2L_2 \times 4L_0$) to match cylinders (having a bulk morphology) both perpendicular to the surfaces and parallel to the x direction (thus the surfaces). In both orientations, $\mathbf{n}_0$ is parallel to the y direction. The observed morphologies are summarized in Table 3.

4.1. Conditions for Perpendicular Cylinders. As shown in Table 3, cylinders perpendicular to the surfaces ($C_\perp$) are readily observed between sB−sB surfaces with a slight preference ($\alpha = 0.2$) for all the surface separations studied in this work. Figure 5a shows a representative configuration of the system between such surfaces separated by $D = 49$ ($1.75L_2$), where hexagonally packed cylinders are perpendicular to the surfaces throughout the film. The box size in the x−y cross section is 28 × 34. In the $C_\perp$ morphology, both A and B segments can be found near the surfaces. This can be

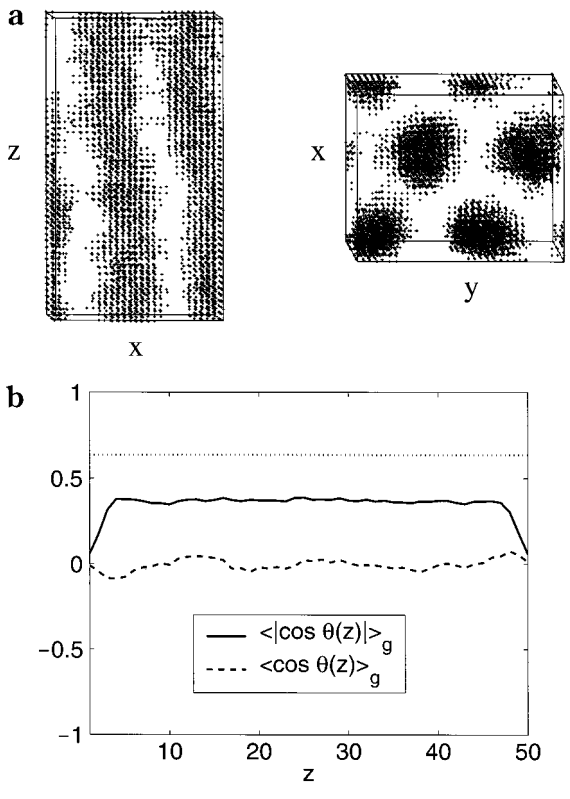

Figure 5. $C_\perp$ morphology between sB−sB surfaces slightly preferring B segments ($D/L_2 = 1.75$, $\alpha = 0.2$). Hexagonally packed cylinders are perpendicular to the surfaces throughout the entire film. (a) Representative configuration of the system. Only A segments are shown as dots. (b) Chain orientation profiles. The dotted line represents the criterion between perpendicular and parallel orientations of the chains, namely $\langle|\cos\theta(z)|\rangle_g = (1/\pi)\int_0^\pi |\cos\theta|\, d\theta = 2/\pi$.

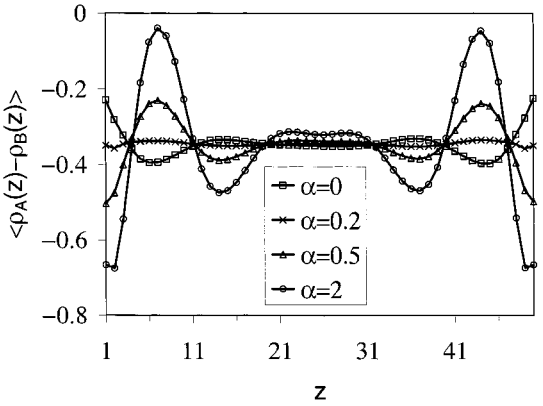

Figure 6. Order parameter profiles between sB−sB surfaces with different strength of preference ($D/L_z = 1.75$). The $C_\perp$ morphology is observed for neutral or weakly preferential surfaces ($\alpha = 0$, 0.2, and 0.5); the $C_{||}-C_\perp-C'_{||}$ morphology is observed for strongly preferential surfaces ($\alpha = 2$).

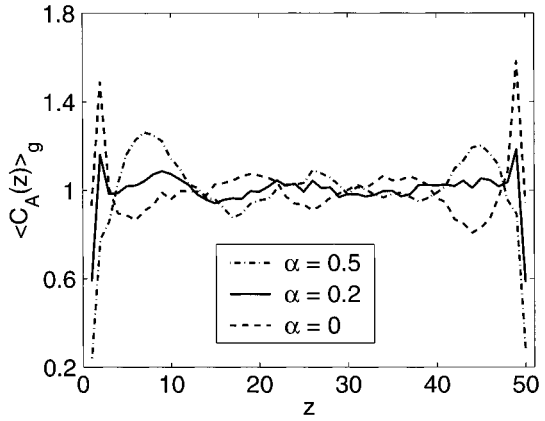

Figure 7. Center-of-mass distribution of A blocks for the $C_\perp$ morphology between sB−sB surfaces with different strength of preference ($D/L_z = 1.75$).

seen from the order parameter profile $\langle \rho_A(z) - \rho_B(z) \rangle$ shown in Figure 6. The almost constant value of −0.35 (for $\alpha = 0.2$) is consistent with the composition of $f_A = {}^1/_4$ and the density of $\langle \rho \rangle \approx 0.7$. That chains are mainly parallel to the surfaces in this morphology is confirmed by the chain orientation profiles shown in Figure 5b. Similar to the case of perpendicular lamellae of symmetric diblock copolymers, the small positive value of $\langle |\cos \theta(z)| \rangle_g$ ($\approx$0.37) in the interior of the film is caused by fluctuations of $\theta(z)$, and the values of almost 0 near the surfaces are due to hard-surface effects (chains whose center-of-mass is close to the surfaces have to orient parallel to the surfaces).[13,30]

As shown in Table 3, perpendicular cylinders are also observed between weakly preferential sB−sB surfaces ($\alpha = 0.5$) and between neutral surfaces ($\alpha = 0$), when $2(D/L_z)$ is half an odd integer. Similar to the case of confined lamellae,[13] these configurations lead to a small or nonexistent surface−block interfacial energy cost when both species are present near the surface, and a strong frustration (i.e., a cost of elastic free energy associated with chain conformational entropy) when parallel cylinders form. Perpendicular cylinders are therefore preferred over parallel cylinders.

As was the case for perpendicular lamellae confined between two weakly preferential surfaces,[13,31] the perpendicular cylinders also exhibit some undulation of the A−B interfaces, as shown in Figure 6. We can see that energetically neutral surfaces ($\alpha = 0$) exhibit a slight preference for A blocks, which are shorter. This can also be seen from the center-of-mass distribution of A blocks shown in Figure 7. In general, due to hard-surface effects,[13] $\langle C_A(z) \rangle_g$ has a smaller value at the surfaces ($z = 1$ and L_z) than its average value of 1 (see the case $\alpha = 0.2$). However, in the case $\alpha = 0$, this is set off by the slight preference of the neutral surfaces for A blocks, and therefore $\langle C_A(1) \rangle_g \approx \langle C_A(L_z) \rangle_g \approx 1$. The slight preference of neutral surfaces for the shorter blocks reported here was also found by Huinink et al. in density functional calculations.[41]

We attribute this effect to the enrichment of chain ends (relative to middle segments) near a hard and flat surface.[57] In the athermal case ($\epsilon_{A-B} = 0$ and $\alpha = 0$), the only difference between A and B segments in *asymmetric* diblock copolymers is that the A segments (the shorter blocks) are on the average closer to a chain end than the B segments (the longer blocks). In other words, the fraction of chain ends of type A is always ${}^1/_2$, larger than the overall composition f_A. The enrichment of chain ends near the surfaces therefore results in a slight preference of neutral surfaces for the shorter blocks. This is a purely entropic effect, and when $\epsilon_{A-B} > 0$, the repulsion between A and B blocks enhances this entropic preference.

When D/L_z is half an integer, the preference of neutral surfaces for A blocks results in the formation of parallel cylinders. The $C_{||}^{1/2}-C_{||}^{1}-C_{||}^{1/2}$ morphology for $D/L_z = 1$ is shown in Figure 8. The box size in the $x-y$ cross section is 28×34. If we ignore surface effects, the morphology shown in Figure 8 would represent a repeat unit of the hexagonally packed cylinders observed in the bulk. In the strong segregation limit (SSL), by assuming a constant density ρ and a *regular*-hexagonal packing of cylinders both in the film and in the bulk, we get the radius of the cylinders $R = R_0 = \sqrt{3}/(8\pi)L_0 \approx 0.2625L_0$ when $f_A = {}^1/_4$ (R_0 denotes the radius of cylinders in the bulk under the above assumptions). Figure 8b compares the order parameter profile obtained in our simulation with that calculated from SSL (where ρ is taken from the simulation); reasonable agreement is obtained between the two. The assumption of vanishingly small A−B interfaces in SSL leads to the flat minima of $\rho_A(z) - \rho_B(z)$. The preference of neutral surfaces for A blocks can be clearly seen by comparing the three local maxima of $\langle \rho_A(z) - \rho_B(z) \rangle$. Figure 8c shows the density profile; the fluctuations are mainly due to the concentration of vacancies near the A−B interfaces, which reduces the block−block interfacial energy of the system. The density decrease at the surfaces ($z = 1$ and L_z) is again a manifestation of the hard-surface effects.[13] Figure 8d−f can be understood by the representative configuration shown in Figure 8a. Note that both parts b and e of Figure 8 show a stronger segregation of A segments near neutral surfaces in this morphology than in perpendicular cylinders (compare to Figures 6 and 7, respectively).

The perpendicular cylinders observed between sA−sA surfaces by Thomas and co-workers[42,45] have been proposed to be metastable.[45] Recently, Thurn-Albrecht et al. observed perpendicular cylinders throughout their 40 nm thick asymmetric diblock copolymer films of poly(styrene)−poly(methyl methacrylate) (PS−PMMA) on nearly neutral substrates.[52] Although the upper free surface in their experiments exhibits a weak preference for PS blocks (the longer blocks),[58] in addition to the

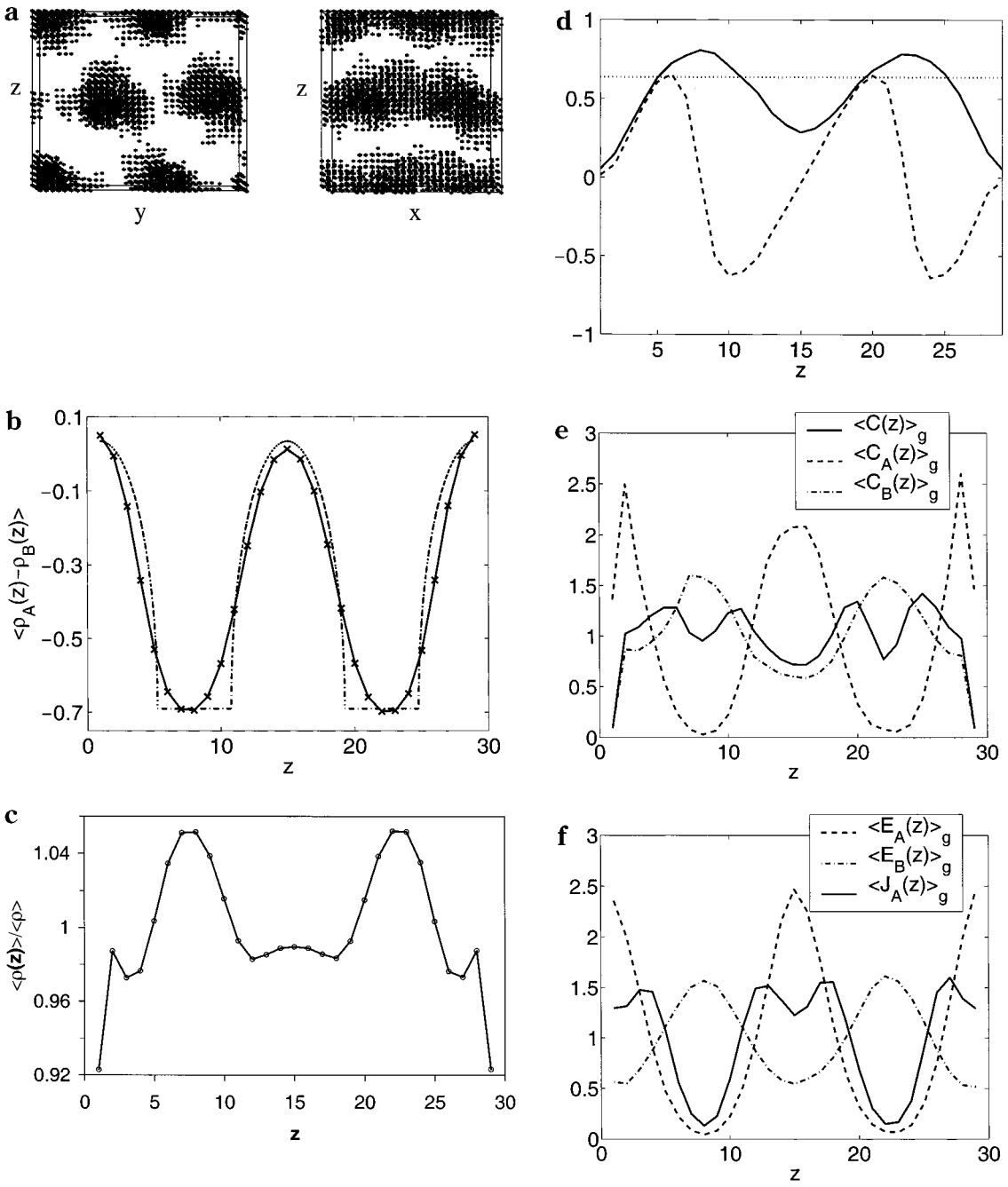

Figure 8. $C_{||}^{1/2}-C_{||}^{1}-C_{||}^{1/2}$ morphology between neutral surfaces separated at $D/L_2 = 1$. One layer of half-cylinders parallel to the surfaces ($C_{||}^{1/2}$) is observed near each surface, and one layer of parallel cylinders ($C_{||}^{1}$) is observed in the interior of the film. The cylinders are hexagonally packed, closely representing a repeat unit of the bulk morphology. (a) Representative configuration of the system. Only A segments are shown as dots. (b) Order parameter profiles obtained from simulations (represented by the symbols connected by a solid line) and calculated from SSL (represented by a dash−dotted line). (c) Density profile. (d) Chain orientation profiles. Refer to Figure 5b for additional information. (e) Center-of-mass distributions. (f) Chain ends and A-joint segments distributions.

nearly neutral substrates the small film thickness (less than L_0) may also prevent the formation of a parallel morphology.

Our conditions for perpendicular cylinders are consistent with the theoretical work of Huinink et al.[41] However, the $C_{||}^{1/2}$ morphology that we observe near neutral surfaces ($\alpha = 0$) when D/L_2 is half an integer is different from the lamellar-like morphology ($L_{||}$) reported by these authors[41] under comparable conditions. In all the $C_{||}^{1/2}$ morphologies that we observe near neutral surfaces, $\langle \rho_A(z) - \rho_B(z) \rangle$ at the surface ($z = 1$ and L_z) has a small positive value similar to that shown in Figure 8b; the $L_{||}$ morphology would result in much larger values (refer to Figure 11).

4.2. Morphologies between sA−sA Surfaces. As shown in Table 3, a surface-induced lamellar ordering is observed when the surfaces have an energetic preference for the shorter (A) blocks. The preferred interfacial curvature toward the majority component (B) is balanced by the energetic surface preference for the minority component (A), leading to a layer of lamellar-like morphology ($L_{||}$) near each surface. (The entropic preference is probably not strong enough to produce $L_{||}$ near a neutral surface.) Note that the A−B interface in the

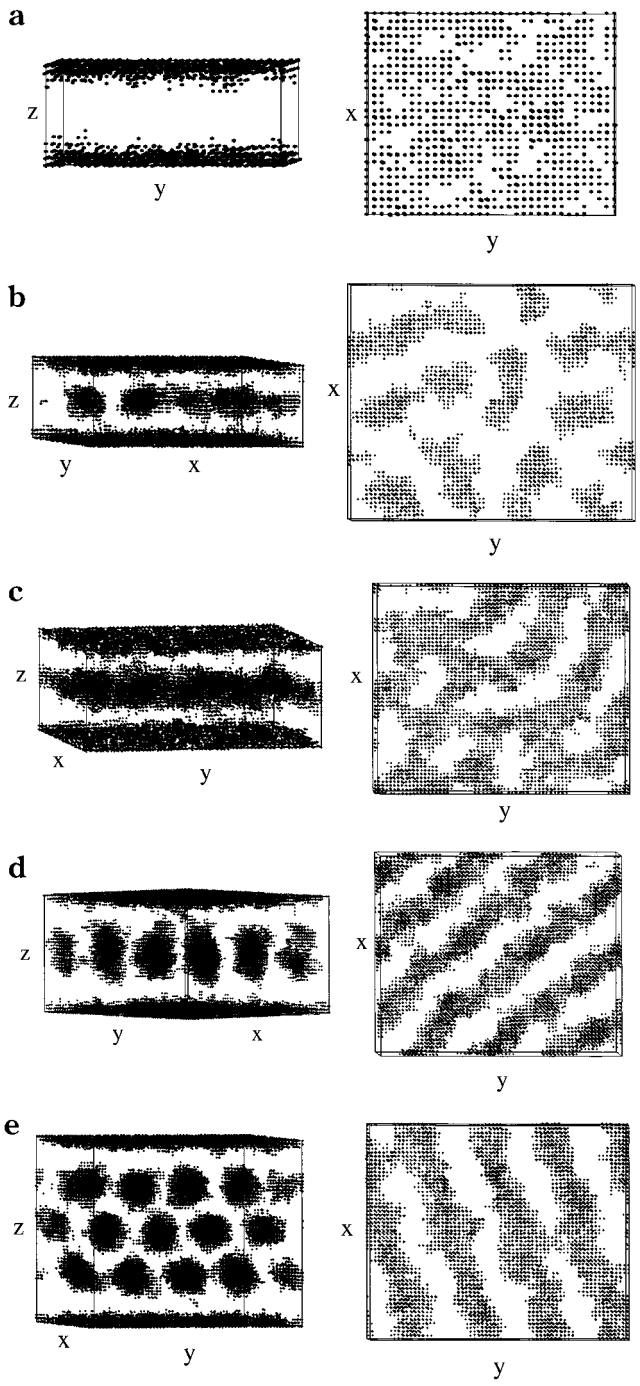

Figure 9. Representative configurations of different morphologies observed between sA−sA surfaces ($\alpha = 2$) with different film thicknesses. Only A segments are shown as dots. (a) $L_{||}-L_{||}$ at $D/L_2 = 0.5$. A morphology of two A−B lamellae ($L_{||}$) is observed. Shown on the right is the upper lamella ($z = 8-15$). (b) $L_{||}-S-L_{||}$ at $D/L_2 = 0.75$. One layer of spherical-like morphology (S) sandwiched between two $L_{||}$ is observed. Shown on the right is the interior of the film ($z = 7-15$). (c) $L_{||}-P-L_{||}$ at $D/L_2 = 1$. One layer of perforated lamellae of A (P) sandwiched between two $L_{||}$ is observed. Shown on the right is the interior of the film ($z = 7-23$). (d) $L_{||}-C_{||}^1-L_{||}$ at $D/L_2 = 1.25$. One layer of parallel cylinders ($C_{||}^1$) sandwiched between two $L_{||}$ is observed. Shown on the right is the interior of the film ($z = 7-30$). The intercylinder distance (parallel to the surfaces) is 14.32, smaller than L_0. (e) $L_{||}-C_{||}^3-L_{||}$ at $D/L_2 = 2$. Three layers of parallel cylinders ($C_{||}^3$) sandwiched between two $L_{||}$ is observed. Shown on the right is the lower layer of the cylinders ($z = 7-21$). The intercylinder distance (parallel to the surfaces) is 16.05, smaller than L_0.

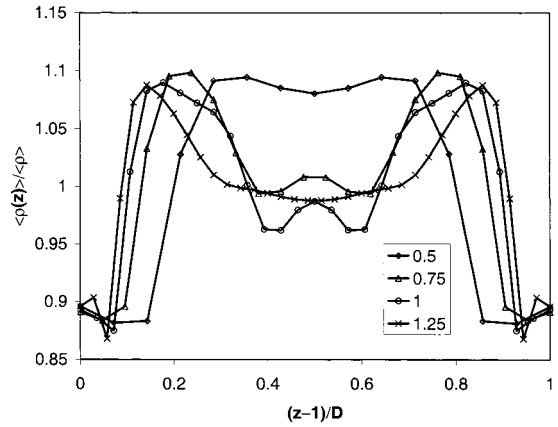

Figure 10. Density profiles of different morphologies (refer to Figure 9) between sA−sA surfaces ($\alpha = 2$). D/L_2 for each case is listed in the legend.

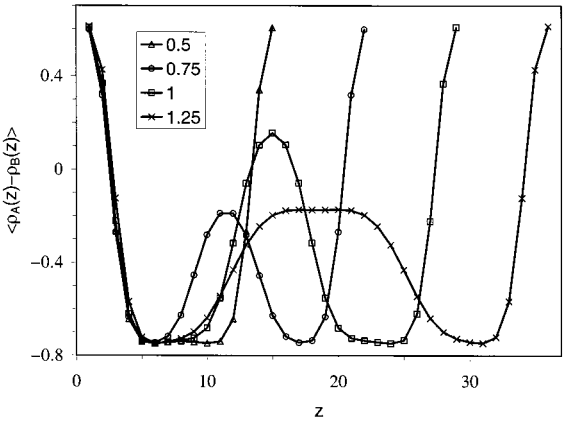

Figure 11. Order parameter profiles of different morphologies (refer to Figure 9) between sA−sA surfaces ($\alpha = 2$). D/L_2 for each case is listed in the legend.

$L_{||}$ morphology is basically a plane parallel to the surfaces. Such a surface-induced morphological transformation has been consistently observed in experiments involving an sA surface[42−49] and was also predicted theoretically by Turner et al.[59]

Depending on the film thickness, different morphologies are observed in the interior of the film sandwiched between two $L_{||}$, as shown in Table 3. Representative configurations of these morphologies for $\alpha = 2$ and different values of D/L_2 are shown in Figure 9a−e. The density profiles and the order parameter profiles for these morphologies, except that in Figure 9e, are shown in Figures 10 and 11, respectively. From Figure 11 we can see that the order parameter profiles near the surfaces are similar, despite different interior morphologies. Since $\langle \rho_A(z) - \rho_B(z) \rangle$ reaches its minima at $z = 6$ and $z = L_z - 5$ in all these cases, we define the regions of $z = 1-6$ and $z = L_z - 5 \sim L_z$ as the surface layers.

Noncylindrical morphologies of lamellae ($L_{||}$) and spheres (S) have been observed in the interior of thin films in some experiments involving two sA surfaces; they have been explained by the (volume fraction) depletion of A segments in the interior of the film caused by the surface-induced segregation of A segments to the surface layers.[46−49] We therefore list in Table 4 the average volume fractions of A segments in the surface layers and in the interior of the films (denoted by f_A^{sl} and f_A^{in}, respectively) for different morphologies (at $\alpha =$

Table 4. Comparison of Volume Fractions of A Segments Averaged in the Surface Layers (f_A^{sl}) and in the Interior of the Film (f_A^{in}) for Different Morphologies between sA−sA Surfaces ($\alpha = 2$)

morphology	D/L_2	f_A^{sl}	f_A^{in}
$L_{\|\|}-L_{\|\|}$	0.5	0.350	0.000
$L_{\|\|}-S-L_{\|\|}$	0.75	0.349	0.176
$L_{\|\|}-P-L_{\|\|}$	1	0.362	0.203
$L_{\|\|}-C_{\|\|}^1-L_{\|\|}$	1.25	0.388	0.202
$L_{\|\|}-C_{\|\|}^2-L_{\|\|}$	1.5	0.368	0.223
$L_{\|\|}-C_{\|\|}^2-L_{\|\|}$	1.75	0.386	0.222
$L_{\|\|}-C_{\|\|}^3-L_{\|\|}$	2	0.369	0.232

2); they are calculated from $f_A(z) \equiv (1 + \langle \rho_A(z) - \rho_B(z)\rangle / \langle \rho(z)\rangle)/2$. We can see that f_A^{sl} is almost constant and is larger than f_A ($=1/4$), while f_A^{in} varies depending on the interior morphologies and is smaller than f_A. This is in agreement with the above explanations.

For $D/L_2 = 0.5$, the film consists of two $L_{||}$ and $f_A^{in} = 0$. This $L_{||}-L_{||}$ morphology is consistent with experimental observations on ultrathin films between two sA surfaces.[42,46−48] The mean-square end-to-end distances for this morphology are listed in Table 2. We can see that the dimensions of A blocks are smaller than in the bulk, in qualitative agreement with experimental measurements.[46] For $D/L_2 = 0.75$, the small value of f_A^{in} results in discontinuous, spherical-like regions of A blocks (S) in the interior of the film. A similar morphology of $L_{||}-S-L_{||}$ has been observed in experiments,[46−48] where spheres of A blocks were hexagonally packed in the matrix of B, constituting the middle layer of the film. The irregular shape and packing of the A-rich regions shown in Figure 9b may be due to the mismatch between PBC (in the $x-y$ cross section of our simulation box, 56×67) and the characteristic periodicity of the hexagonal packing of spheres (which is unknown). For $D/L_2 = 1$, a larger value of f_A^{in} leads to the interior morphology of perforated lamellae of A blocks (P). Again, the irregular shape and packing of the B-rich holes in the perforated lamellae shown in Figure 9c may be due to the mismatch between the PBC and the characteristic periodicity of the hexagonal packing of these holes. Figure 11 shows that, different from the above two cases, $\langle \rho_A(z) - \rho_B(z)\rangle > 0$ in the middle of the film for the P morphology. This suggests that the formation of P result from the *local* depletion of B segments in the middle of the film. This can be further understood in section 4.3, where the P morphology is observed between sB−sB surfaces with $D/L_2 = 0.5$.

Interestingly, for a thicker film of $D/L_2 = 1.25$, a similar value of f_A^{in} leads to an interior morphology consisting of one layer of parallel cylinders of A blocks ($C_{||}^1$). The intercylinder distance $L \approx 14.3$, however, is smaller than L_0. In addition, $\langle \rho_A(z) - \rho_B(z)\rangle$ in the middle of the film (at $z = 18$ and 19) is less than the corresponding value in the $C_{||}^{1/2}-C_{||}^1-C_{||}^{1/2}$ morphology shown in Figure 8b; the radius of the cylinders R (estimated under the assumptions of SSL) is therefore smaller than the bulk value R_0. These trends are consistent with experimental measurements.[42,46] We also note from Figures 9d and 11 that the cylinder layer is somewhat elongated along the z direction by the incommensurate surface separation D/L_2. For the thicker films in this study, larger values of f_A^{in} (as shown in Table 4) lead to interior morphologies of hexagonally packed parallel cylinders with an intercylinder distance $L \approx 16.05$, which are closer to the cylindrical bulk morphology than in the case $D/L_2 = 1.25$. The decrease of L from L_0 in thin films will be discussed further in section 4.3. Similar $L_{||}-C_{||}^n-L_{||}$ morphologies have also been observed in experiments involving two sA surfaces.[42,43,45−49]

4.3. Morphologies between sB−sB Surfaces. As shown in Table 3, when the majority component (B) is preferred by the surfaces, our simulations do not provide any evidence of a surface-induced lamellar-like morphology having a *planar* A−B interface parallel to the surfaces ($L_{||}$). We explain this by considering the following two facts: First, in the above case of sA−sA surfaces, the preferred interfacial curvature (toward B) brings B blocks toward the surfaces, which is energetically unfavorable. In the case of sB−sB surfaces, the preferred interfacial curvature brings A blocks away from the surfaces, which is energetically favorable. Second, B blocks are much longer than A blocks; since the surface−block interactions are short-ranged, the energetic surface preference is less effective than in the case of sA−sA surfaces. Therefore, the preferred interfacial curvature is preserved. Our observations are consistent with all the experiments reported so far involving an sB surface.[44,46−48,53] Note that previous theoretical studies[16,41,59] contradict experimental evidence in that they predict surface-induced lamellar-like structures near sB surfaces.

As shown in Table 3, the morphologies of A-rich perforated lamellae between B-rich layers (P for $D/L_2 = 0.5$ and P−P for $D/L_2 = 1$) are observed in thin films between sB−sB surfaces. They are shown in Figure 12 for $\alpha = 2$. As in the case of $L_{||}-P-L_{||}$ shown in Figure 9c, the irregular shape and packing of the B-rich holes in the perforated lamellae shown in Figure 12a,b may also be due to the mismatch between the PBC and the characteristic periodicity of the hexagonal packing of these holes. The common features of $\langle \rho(z)\rangle/\langle \rho\rangle < 1$ and $\langle \rho_A(z) - \rho_B(z)\rangle > 0.15$ (for $\alpha = 2$) in the middle of each P layer in all these cases help us identify the morphologies. The formation of P results from the surface-induced segregation of B blocks to the surfaces, which causes a depletion of B segments in the interior of the film. Similar morphologies were observed in experiments involving identical sB−sB surfaces, where the holes were described as channels of B blocks connecting the upper and lower B-rich layers.[46] The mean-square end-to-end distances for the P morphology are listed in Table 2. We can see that the dimensions of B blocks are smaller than in the bulk, again in qualitative agreement with experimental measurements.[46] Note that Huinink et al.[41] also observed the P morphology in their theoretical calculations under similar conditions, whereas $L_{||}-L_{||}$ and $C_{||}^1$ were reported for slightly different conditions.

Parallel cylinders are observed for thicker films, with D/L_2 being half an integer, and for weaker surface preferences, where the depletion of B segments in the interior of the film is less significant. Figure 13 shows the $C_{||}^3$ morphology for $D/L_2 = 1.5$ and $\alpha = 2$. We can see that the surface-induced segregation of B blocks results in higher values of $\langle \rho_A(z) - \rho_B(z)\rangle$ at the centers of the cylinder layers near the surfaces (≈ 0.10 at $z = 8$ and 36) than at the center of the middle layer (at $z = 22$). Consequently, the cylinder layers near the surfaces exhibit some features toward the P morphology. In addition, the unusual behavior of $\langle \rho_A(z) - \rho_B(z)\rangle$ near the surfaces (at $z = 1$ and $z = L_z$) has been observed for

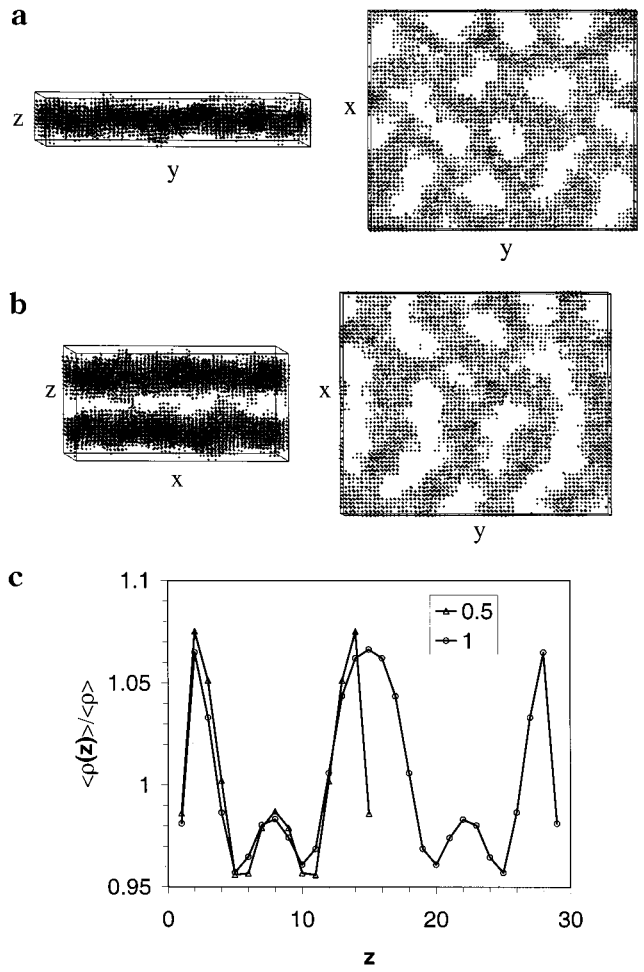

Figure 12. P morphology (for $D/L_2 = 0.5$) and P−P morphology (for $D/L_2 = 1$) between sB−sB surfaces with $\alpha = 2$. A-rich perforated lamellae between B-rich layers are observed. (a) Representative configuration of the system for the P morphology. Only A segments are shown as dots. (b) Representative configuration of the system for the P−P morphology. Only A segments are shown as dots. Shown on the right is the lower layer of the perforated lamellae ($z = 1-15$). (c) Density profiles. D/L_2 for each case is listed in the legend.

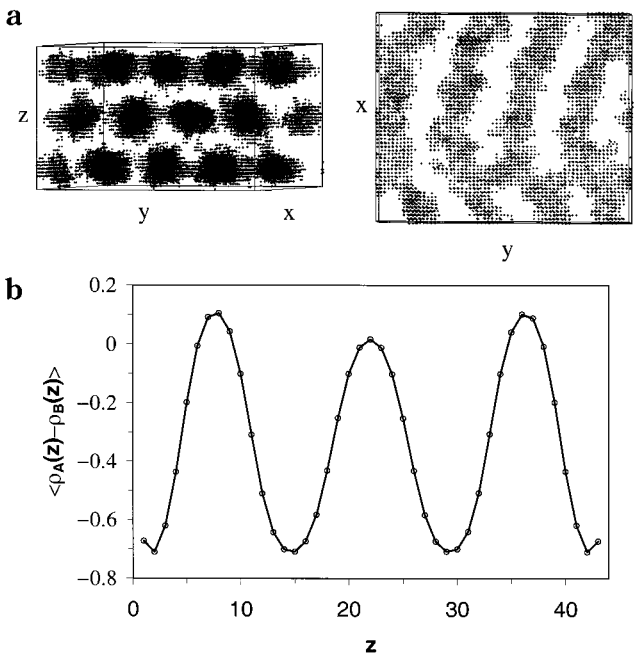

Figure 13. $C_{||}^3$ morphology between sB−sB surfaces ($\alpha = 2$) separated at $D/L_2 = 1.5$. Three layers of hexagonally packed parallel cylinders are observed. The intercylinder distance (parallel to the surfaces) is 16.05, smaller than L_0. (a) Representative configuration of the system. Only A segments are shown as dots. Shown on the right is the upper layer of cylinders ($z = 29-43$). (b) Order parameter profile.

most morphologies between sB−sB surfaces in our simulations; we attribute it to the entropic preference of the hard surfaces for the shorter (A) blocks. Our conditions for the formation of the $C_{||}^n$ morphology with $n \geq 2$ are consistent with the theoretical calculations of Huinink et al.[41] Parallel cylinders between sB−sB surfaces have also been observed in experiments.[46]

Similar to the cases of $L_{||}-C_{||}^n-L_{||}$ between sA−sA surfaces, we note that for this $C_{||}^3$ morphology the intercylinder distance $L \approx 16.05$ is smaller than L_0. As shown in Table 3, the surface-induced segregation of one block could reduce the intercylinder distance L of parallel cylinders. Since the available "options" for L of parallel cylinders (in the cross section of our simulation box, 56×67) are rather limited (the only "options" between 14 and 17 are 16.75 ($\approx L_0$), 16.306 11, 16.047 53, 14.374 32, 14.322 59, and 14), the values of L shown in Table 3 only provide a general trend: the stronger the surface-induced segregation, the larger the decrease of L from L_0. More accurate determination of L for each case would require larger simulation boxes and more simulation runs. Such studies, however, are beyond the scope of this work.

When $2(D/L_2)$ is half an odd integer, the $C_{||}^n$ morphology would be strongly frustrated; cylinders therefore orient perpendicular to the surfaces to preserve the dimensions and hexagonal packing in the bulk. However, in contrast to the case of weak surface preference ($\alpha = 0.5$) where $C_\perp$ forms throughout the film, at a small distance away from the surfaces the depletion of B segments (caused by a stronger surface preference $\alpha =$ 1 or 2) results in the interconnection of A domains to form parallel cylinders. Such a morphology, denoted by $C_{||}-C_\perp-C_{||}'$, is shown in Figure 14 for $D/L_2 = 1.75$ and $\alpha = 2$. The orientations of the upper and lower parallel cylinders do not have to be the same, since for *regular*-hexagonally packed perpendicular cylinders the three different orientations of the parallel cylinders (resulting from the interconnection of the nearest A domains) have the same L. However, due to the dimensions of the simulation box in the cross section parallel to the surfaces (28×34), the different orientations of $C_{||}$ and $C_{||}'$ actually lead to a small difference in L of the parallel cylinders shown in Figure 14b,d. Comparison of the order parameter profiles for $\alpha = 0.5$ ($C_\perp$) and $\alpha = 2$ ($C_{||}-C_\perp-C_{||}'$) shown in Figure 6 highlights the effects of the stronger surface preference.

The $C_{||}-C_\perp-C_{||}'$ morphology results from both the hard surface confinement and the relatively strong surface preference. Since experiments have been limited to films with at least one free surface, it has not been observed experimentally. Neither was it observed in previous dynamic density functional calculations,[41] possibly because the range of surface preferences studied in that work was small.

5. Concluding Remarks

We have performed extensive Monte Carlo simulations for thin films of asymmetric diblock copolymers

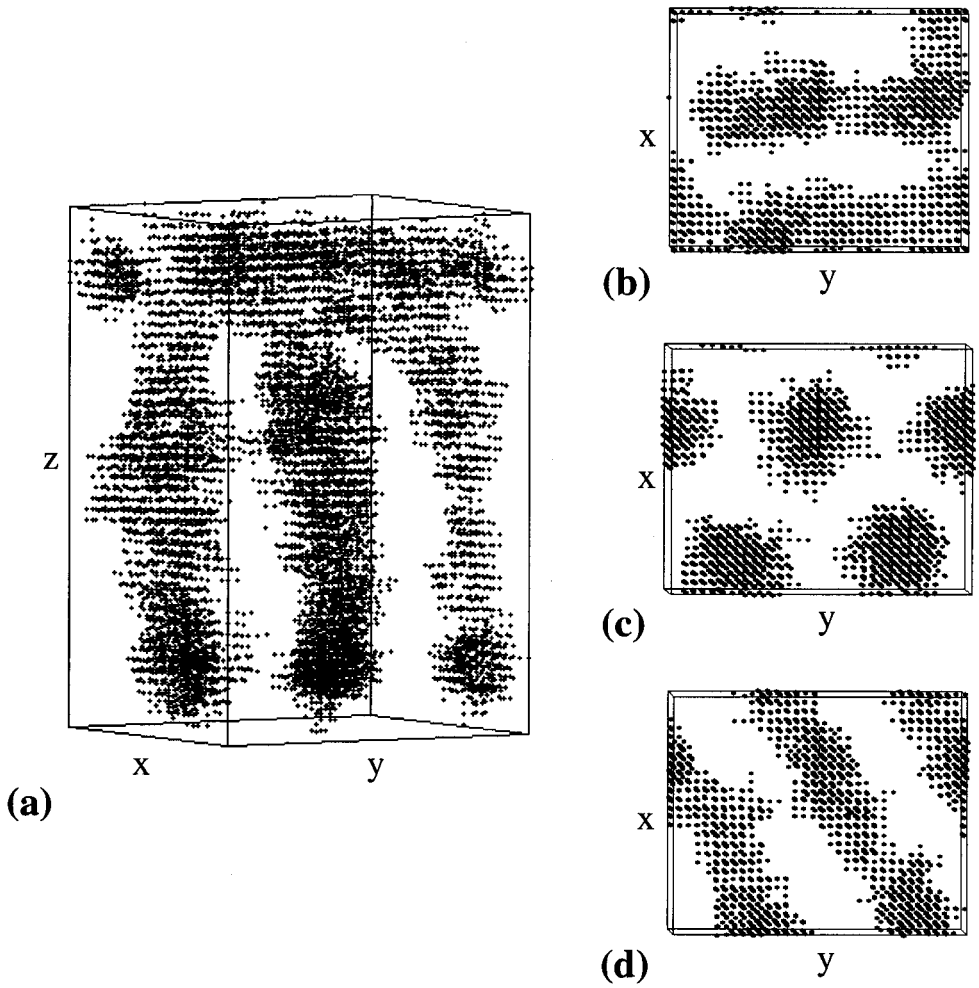

Figure 14. Representative configuration of the $C_{\parallel}-C_{\perp}-C'_{\parallel}$ morphology observed between sB−sB surfaces ($\alpha = 2$) separated at $D/L_2 = 1.75$. Only A segments are shown as dots. Perpendicular cylinders ($C_{\perp}$) are observed in the interior of the film. One layer of parallel cylinders with intercylinder distance of 14.53 ($C_{\parallel}$) is observed near the lower surface, and another layer of parallel cylinders with intercylinder distance of 14 ($C'_{\parallel}$) is observed near the upper surface. $C_{\parallel}$ and $C'_{\parallel}$ are formed by interconnecting the nearest A domains in $C_{\perp}$. (a) Side view (parallel to the surfaces) of the whole film. (b) Top view (perpendicular to the surfaces) of $C'_{\parallel}$ ($z = 36-50$). (c) Top view of $C_{\perp}$ ($z = 16-35$). (d) Top view of $C_{\parallel}$ ($z = 1-15$).

confined between two homogeneous and identical surfaces. Our simulations have been performed in an expanded grand-canonical ensemble in the framework of a simple cubic lattice. The confined films are in thermodynamic equilibrium with a bulk phase having the same chemical potential and temperature. We have studied systematically the morphological dependence of the thin films on the surface−block interactions and the film thickness. Overall, our results are in good qualitative agreement with the experimental observations summarized in Table 1.

In the bulk, the asymmetric diblock copolymers form cylinders consisting of the minority component (A) in a matrix of the majority component (B). These cylinders are arranged in a hexagon, forming a two-dimensional periodic pattern. To reduce finite size effects caused by the hexagonal packing of the cylinders and the periodic boundary conditions imposed by the simulation box, it is necessary to match the box dimensions with the characteristic periodicity of the pattern. We have therefore performed exploratory bulk simulations with judicious choices of the box dimensions to find the characteristic periodicity of the cylinders in the bulk.

For confined films, the preference of the surfaces and the film thickness determine the morphology of the asymmetric diblock copolymers. We have found that energetically neutral surfaces ($\alpha = 0$) exhibit a slight entropic preference for the *shorter* blocks, due to the enrichment of chain ends near hard surfaces. Perpendicular cylinders are readily observed between two hard surfaces having a slight energetic preference for the *longer* blocks, which sets off the entropic preference. Parallel cylinders are observed when the surface preference for the longer blocks becomes stronger. The frustration between the film thickness D and the characteristic length of the hexagonally arranged cylinders in the bulk L_2 (defined in Figure 3) plays an important role on the orientation of confined cylinders, as shown in Table 3. Noncylindrical morphologies, including lamellae, spheres, and perforated lamellae, have also been observed in confined films. These morphologies result from the depletion of the preferred segments (by the surfaces) in the interior of the film. Particularly, we have observed one layer of A−B lamella having a planar A−B interface near surfaces energetically preferring the *shorter* blocks, but not near surfaces energetically preferring the *longer* blocks; this is consistent with all the experimental reports summarized in Table 1. Further simulations with larger boxes are suggested to better resolve the irregularity of the spheres and the perforated lamellae observed in this work.

Our simulations suggest that hexagonally packed perpendicular cylinders can be obtained by finely tuning the surface−block interactions and the film thickness. It has been reported that the orientation of cylinders in thin films can also be controlled by imposing electric fields.[52,60−62] Note, however, that the long-range ordering (in the plane of the film) of perpendicular cylinders cannot be achieved by the use of homogeneous surfaces or electric fields. For some applications (e.g., addressable arrays in storage devices), perfection of the hexagonal packing of the cylinders and the registration of the pattern with a substrate is desirable; a patterned substrate rather than a homogeneous one may therefore be employed. We have demonstrated the feasibility of using a stripe-patterned surface to induce the formation of long-range ordered perpendicular lamellae of symmetric diblock copolymers that are registered with the surface pattern;[28,30,31] further studies on using patterned surfaces to enhance the perfection and the registration of perpendicular cylinders are underway.

Acknowledgment. Financial support for this work was provided by the Semiconductor Research Corporation through Contract 99-LP-452 and by the NSF CTS-9703207 and CTS-9901430.

References and Notes

(1) Bates, F. S.; Fredrickson, G. H. *Annu. Rev. Phys. Chem.* **1990**, *41*, 525.
(2) See, for example: (a) Park, M.; Harrison, C.; Chaikin, P. M.; Register, R. A.; Adamson, D. H. *Science* **1997**, *276*, 1401. (b) Hashimoto, T.; Tsutsumi, K.; Funaki, Y. *Langmuir* **1997**, *13*, 6869. (c) Liu, G.; Ding, J.; Hashimoto, T.; Kimishima, K.; Winnik, F. M.; Nigam, S. *Chem. Mater.* **1999**, *11*, 2233. (d) Lammertink, R. G. H.; Hempenius, M. A.; van den Enk, J. E.; Chan, V. Z.-H.; Thomas, E. L.; Vancso, G. J. *Adv. Mater.* **2000**, *12*, 98. (e) Boontongkong, Y.; Cohen, R. E.; Rubner, M. F. *Chem. Mater.* **2000**, *12*, 1628. (f) Peters, R. D.; Yang, X. M.; Wang, Q.; de Pablo, J. J.; Nealey, P. F. *J. Vac. Sci. Technol. B* **2000**, *18*, 3530.
(3) Lambooy, P.; Russell, T. P.; Kellogg, G. J.; Mayes, A. M.; Gallagher, P. D.; Satija, S. K. *Phys. Rev. Lett.* **1994**, *72*, 2899.
(4) Russell, T. P.; Lambooy, P.; Kellogg, G. J.; Mayes, A. M. *Physica B* **1995**, *213&214*, 22.
(5) Koneripalli, N.; Singh, N.; Levicky, R.; Bates, F. S.; Gallagher, P. D.; Satija, S. K. *Macromolecules* **1995**, *28*, 2897.
(6) Kellogg, G. J.; Walton, D. G.; Mayes, A. M.; Lambooy, P.; Russell, T. P.; Gallagher, P. D.; Satija, S. K. *Phys. Rev. Lett.* **1996**, *76*, 2503.
(7) Koneripalli, N.; Levicky, R.; Bates, F. S.; Ankner, J.; Kaiser, H.; Satija, S. K. *Langmuir* **1996**, *12*, 6681.
(8) Huang, E.; Russell, T. P.; Harrison, C.; Chaikin, P. M.; Register, R. A.; Hawker, C. J.; Mays, J. *Macromolecules* **1998**, *31*, 7641.
(9) Kikuchi, M.; Binder, K. *J. Chem. Phys.* **1994**, *101*, 3367.
(10) Sommer, J. U.; Hoffmann, A.; Blumen, A. *J. Chem. Phys.* **1999**, *111*, 3728.
(11) Geisinger, T.; Muller, M.; Binder, K. *J. Chem. Phys.* **1999**, *111*, 5241.
(12) Geisinger, T.; Muller, M.; Binder, K. *J. Chem. Phys.* **1999**, *111*, 5251.
(13) Wang, Q.; Yan, Q.; Nealey, P. F.; de Pablo, J. J. *J. Chem. Phys.* **2000**, *112*, 450.
(14) Shull, K. R. *Macromolecules* **1992**, *25*, 2122.
(15) Turner, M. S. *Phys. Rev. Lett.* **1992**, *69*, 1788.
(16) Brown, G.; Chakrabarti, A. *J. Chem. Phys.* **1994**, *101*, 3310.
(17) Wong, K. Y.; Trache, M.; McMullen, W. E. *J. Chem. Phys.* **1994**, *101*, 5372.
(18) Walton, D. G.; Kellogg, G. J.; Mayes, A. M.; Lambooy, P.; Russell, T. P. *Macromolecules* **1994**, *27*, 6225.
(19) Brown, G.; Chakrabarti, A. *J. Chem. Phys.* **1995**, *102*, 1440.
(20) Turner, M. S.; Johner, A.; Joanny, J.-F. *J. Phys. I* **1995**, *5*, 917.
(21) Milner, S. T.; Morse, D. C. *Phys. Rev. E* **1996**, *54*, 3793.
(22) Matsen, M. W. *J. Chem. Phys.* **1997**, *106*, 7781.
(23) Pickett, G. T.; Balazs, A. C. *Macromolecules* **1997**, *30*, 3097.
(24) Tang, W. H. *Macromolecules* **2000**, *33*, 1370.
(25) Morgado, W. A. M.; Martins, S.; Bahiana, M.; Massunaga, M. S. O. *Physica A* **2000**, *283*, 208.
(26) Fasolka, M. J.; Banerjee, P.; Mayes, A. M.; Pickett, G.; Balazs, A. C. *Macromolecules* **2000**, *33*, 5702.
(27) Rockford, L.; Liu, Y.; Mansky, P.; Russell, T. P.; Yoon, M.; Mochrie, S. G. J. *Phys. Rev. Lett.* **1999**, *82*, 2602.
(28) Yang, X. M.; Peters, R. D.; Nealey, P. F.; Solak, H. H.; Cerrina, F. *Macromolecules* **2000**, *33*, 9575.
(29) Rockford, L.; Mochrie, S. G. J.; Russell, T. P. *Macromolecules* **2001**, *34*, 1487.
(30) Wang, Q.; Yan, Q.; Nealey, P. F.; de Pablo, J. J. *Macromolecules* **2000**, *33*, 4512.
(31) Wang, Q.; Nath, S. K.; Graham, M. D.; Nealey, P. F.; de Pablo, J. J. *J. Chem. Phys.* **2000**, *112*, 9996.
(32) Halperin, A.; Sommer, J. U.; Daoud, M. *Europhys. Lett.* **1995**, *29*, 297.
(33) Petera, D.; Muthukumar, M. *J. Chem. Phys.* **1997**, *107*, 9640.
(34) Chen, H.; Chakrabarti, A. *J. Chem. Phys.* **1998,** *108*, 6897.
(35) Petera, D.; Muthukumar, M. *J. Chem. Phys.* **1998**, *109*, 5101.
(36) Chakrabarti, A.; Chen, H. *J. Polym. Sci., Part B: Polym. Phys.* **1998**, *36*, 3127.
(37) Pereira, G. G.; Williams, D. R. M. *Macromolecules* **1999**, *32*, 758.
(38) Nath, S. K.; Nealey, P. F.; de Pablo, J. J. *J. Chem. Phys.* **1999**, *110*, 7483.
(39) Pereira, G. G.; Williams, D. R. M.; Chakrabarti, A. *J. Chem. Phys.* **2000**, *112*, 10011.
(40) Suh, K. Y.; Kim, Y. S.; Lee, H. H. *J. Chem. Phys.* **1998**, *108*, 1253.
(41) Huinink, H. P.; Brokken-Zijp, J. C. M.; van Dijk, M. A.; Sevink, G. J. A. *J. Chem. Phys.* **2000**, *112*, 2452.
(42) Henkee, C. S.; Thomas, E. L.; Fetters, L. J. *J. Mater. Sci.* **1988**, *23*, 1685.
(43) Karim, A.; Singh, N.; Sikka, M.; Bates, F. S.; Dozier, W. D.; Felcher, G. P. *J. Chem. Phys.* **1994**, *100*, 1620.
(44) Liu, Y.; Zhao, W.; Zheng, X.; King, A.; Singh, A.; Rafailovich, M. H.; Sokolov, J.; Dai, K. H.; Kramer, E. J.; Schwarz, S. A.; Gebizlioglu, O.; Sinha, S. K. *Macromolecules* **1994**, *27*, 4000.
(45) Mansky, P.; Chaikin, P.; Thomas, E. L. *J. Mater. Sci.* **1995**, *30*, 1987.
(46) Radzilowski, L. H.; Carvalho, B. L.; Thomas, E. L. *J. Polym. Sci., Part B: Polym. Phys.* **1996**, *34*, 3081.
(47) Park, M.; Harrison, C.; Chaikin, P. M.; Register, R. A.; Adamson, D.; Yao, N. *Mater. Res. Soc. Symp. Proc.* **1997,** *461*, 179.
(48) Harrison, C.; Park, M.; Chaikin, P. M.; Register, R. A.; Adamson, D. H.; Yao, N. *Polymer* **1998**, *39*, 2733.
(49) Harrison, C.; Park, M.; Chaikin, P.; Register, R. A.; Adamson, D. H.; Yao, N. *Macromolecules* **1998**, *31*, 2185.
(50) Lammertink, R. G. H.; Hempenius, M. A.; Vancso, G. J. *Langmuir* **2000**, *16*, 6245.
(51) Lammertink, R. G. H.; Hempenius, M. A.; Vancso, G. J.; Shin, K.; Rafailovich, M. H.; Sokolov, J. *Macromolecules* **2001**, *34*, 942.
(52) Thurn-Albrecht, T.; Steiner, R.; DeRouchey, J.; Stafford, C. M.; Huang, E.; Bal, M.; Tuominen, M.; Hawker, C. J.; Russell, T. P. *Adv. Mater.* **2000**, *12*, 787.
(53) Although the $L_{||}$ morphology (consisting of only one A−B lamella) was observed between sB−sA surfaces for ultrathin films (15 nm),[47] it is actually caused by the upper sA surface and the very small film thickness (the intercylinder distance is 27 nm for the cylinders in thin films of the diblock copolymers studied[48]); for thicker films no $L_{||}$ was observed near an sB surface.[47]
(54) Escobedo, F. A.; de Pablo, J. J. *J. Chem. Phys.* **1996**, *105*, 4391.
(55) Binder, K.; Fried, H. *Macromolecules* **1993**, *26*, 6878.
(56) Micka, U.; Binder, K. *Macromol. Theory Simul.* **1995**, *4*, 419.
(57) See, for example: Wang, J. S.; Binder, K. *J. Phys. I* **1991**, *1*, 1583 and references therein.
(58) Huang, E.; Mansky, P.; Russell, T. P.; Harrison, C.; Chaikin, P. M.; Register, R. A.; Hawker, C. J.; Mays, J. *Macromolecules* **2000**, *33*, 80.
(59) Turner, M. S.; Rubinstein, M.; Marques, C. M. *Macromolecules* **1994**, *27*, 4986.
(60) Morkved, T. L.; Lu, M.; Urbas, A. M.; Ehrichs, E. E.; Jaeger, H. M.; Mansky, P.; Russell, T. P. *Science* **1996**, *273*, 931.
(61) Mansky, P.; DeRouchey, J.; Russell, T. P.; Mays, J.; Pitsikalis, M.; Morkved, T.; Jaeger, H. *Macromolecules* **1998**, *31*, 4399.
(62) Thurn-Albrecht, T.; DeRouchey, J.; Russell, T. P.; Jaeger, H. M. *Macromolecules* **2000**, *33*, 3250.

MA0018751